Spatial Zadoff-Chu modulation for rapid beam alignment in mmWave phased arrays

Nitin Jonathan Myers, Amine Mezghani and Robert W. Heath Jr.
Department of Electrical and Computer Engineering
The University of Texas at Austin
Email: {nitinjmyers, amine.mezghani, rheath}@utexas.edu

***Abstract*—Compressed sensing (CS) algorithms can be used to perform beam alignment in mmWave phased arrays with fewer channel measurements by exploiting the sparsity of mmWave channels. Unfortunately, several efficient CS matrices cannot be realized in phased arrays due to hardware constraints. In this work, we propose to use shifted Zadoff-Chu (ZC) sequences in the antenna domain to realize efficient CS matrices for channel estimation or beam alignment. We prove that the shifted ZC-based CS matrix satisfies the restricted isometry property with high probability. Furthermore, CS algorithms that use the proposed training can exploit the fast Fourier transform and are computationally efficient over those that use pseudo-random phase shifts. Using simulations, we show that the proposed CS matrix achieves better beam alignment performance than the commonly used random phased shift-based CS matrices.**

***Index Terms*—Spatial Zadoff-Chu modulation, convolutional compressed sensing, analog beamforming, channel estimation**

I. Introduction

To achieve sufficient link margin at the receiver, mmWave systems use large antenna arrays [1]. Directional beamforming using phased arrays is one way to use the large arrays in these systems [2]. Configuring the phased array, however, is challenging in large antenna systems as the best beams have to be estimated under strict hardware constraints [2]. For instance, the use of a single radio frequency chain in a phased array limits the number of channel measurements to one-per-symbol duration. The channel measurements can only be obtained by changing the phase of the signals associated with each antenna. Furthermore, the resolution of the phase control is limited in practice. The strict hardware constraints imposed by phased arrays complicate the beam alignment problem in mmWave systems.

Compressed sensing [3] is valuable in mmWave systems as it can reduce the overhead required for beam alignment when compared to exhaustive beamscanning [2]. As mmWave MIMO channels are approximately sparse in the angle domain [4], several CS-based algorithms have been proposed for channel estimation and beam alignment with fewer channel measurements compared to the channel dimensions [5][6]. Prior work on CS-based beam alignment has used random phase shifts to obtain channel measurements in phased arrays [5] [7]. Although the resultant CS matrices work in practice, it is possible that structured CS matrices may reduce complexity of CS algorithms and improve the beam alignment performance.

Prior work has considered the acquisition of sparse signals using structured CS matrices via convolutional compressed sensing (CCS) [8]. Most CCS techniques acquire signals that are sparse in their canonical representation using circulant shifts of a modulation sequence [9] [10]. In mmWave phased arrays, however, the signal to be acquired using CCS is not sparse in the canonical representation. Instead, it is sparse in the Fourier representation. Vector CCS of signals that are sparse in the canonical or Fourier representations, and the use of Zadoff-Chu sequences [11] in vector CCS were studied in [8]. Unfortunately, the vector CCS technique in [8] cannot be applied to perform simultaneous transmit and receive beam alignment due to the rank-one constraint imposed by the channel acquisition system.

We propose a novel convolutional CS framework that uses shifted versions of a Zadoff-Chu sequence in the antenna domain to acquire spatial channel measurements using the phased array. We show that the beam alignment problem with convolutional channel measurements can be transformed to a Fourier CS problem [12]. We use ideas from Fourier CS to prove that the CS matrix that results from the use of shifted-ZC sequences satisfies the restricted isometry property (RIP) [3]. The RIP is a metric that is used to characterize the efficiency of CS matrices in sparse recovery [3]. Designing CS matrices that satisfy the RIP and are compatible with phased arrays, however, is challenging [8]. We leverage the structure in the transformed CS matrix to develop low-complexity CS algorithms that exploit the fast Fourier transform. Using simulations, we show that CS algorithms that use the proposed CS matrix achieve better beam alignment performance than the commonly used random phase shift-based CS matrices. Note that the matrix CCS framework proposed in this work is not the same as CCS of the vectorized version of a matrix.

Notation: $\mathbf{P}$ is a matrix, $\mathbf{p}$ is a column vector and p is a scalar. The matrices $\mathbf{P}^T$ and $\mathbf{P}^*$ denote the transpose and the conjugate transpose of $\mathbf{P}$. We use $\mathrm{diag}\,(\mathbf{p})$ to denote a diagonal matrix with entries of $\mathbf{p}$ on its diagonal. The m^{th} element of $\mathbf{p}$ is $p[m]$. The Hadamard product of $\mathbf{P}$ and $\mathbf{Q}$ is denoted by $\mathbf{P} \odot \mathbf{Q}$. The Frobenius norm of $\mathbf{P}$ is denoted by $\|\mathbf{P}\|_F$, and the absolute value of p by $|p|$. The matrix $\mathbf{U}_N \in \mathbb{C}^{N \times N}$ denotes the unitary Discrete Fourier Transform (DFT) matrix. The set $\mathcal{I}_N$ denotes the set of integers $\{0, 1, 2, ..., N-1\}$. For $k \in \mathcal{I}_N$, we use $\mathbf{e}_k$ to represent the $(k+1)^{\mathrm{th}}$ canonical basis vector in $\mathbb{C}^N$. The natural logarithm of p is $\log(p)$.

II. System model

The idea underlying our CS matrix design is best understood by considering a narrowband mmWave MIMO system. We extend our design to the wideband case in Sec. V and provide simulations for a practical mmWave setting in Sec. VI.

We consider a point-to-point link with a uniform linear array of N_{tx} antennas at the transmitter (TX) and N_{rx} antennas at the receiver (RX). Both the TX and the RX are equipped with a phased array architecture. The antennas at the TX and RX are connected to their corresponding RF chain through a network of digitally controlled phase shifters as shown in Fig. 1. We assume that the phase shifters at the TX and the RX have resolutions of q_{tx} and q_{rx} bits. The set of allowed phase shifts at the TX is given by $\mathbb{Q}_{\text{tx}} = \left\{e^{\text{j}\beta_{\text{tx}}(1)}, e^{\text{j}\beta_{\text{tx}}(2)}, ..., e^{\text{j}\beta_{\text{tx}}(2^{q_{\text{tx}}})}\right\}$ where $\beta_{\text{tx}}(k) = 2\pi k/2^{q_{\text{tx}}}$. Similarly, the set $\mathbb{Q}_{\text{rx}}$ is defined for phase control over the phase shifters at the RX. We use $\mathbf{H} \in \mathbb{C}^{N_{\text{rx}} \times N_{\text{tx}}}$ to denote the MIMO channel matrix between the TX and the RX. In this work, a sparse approximation of the channel matrix in the Fourier domain is estimated and used for beam alignment.

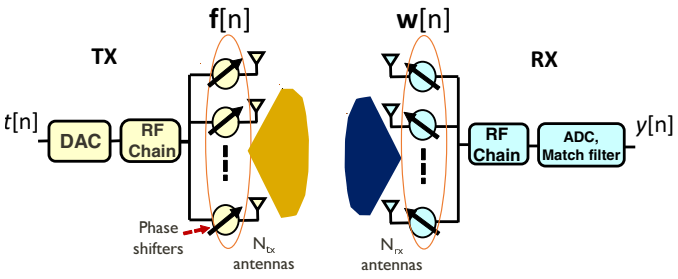

Fig. 1. A MIMO system with phased arrays at the TX and the RX. Channel measurements are acquired by applying different weights to the phased arrays.

The TX transmits a sequence of N_{p} pilot symbols $\{t[n]\}_{n=1}^{N_{\text{p}}}$ into the wireless channel. Each of the pilot symbols is assumed to be unit norm, i.e., $|t[n]| = 1$. For the n^{th} pilot transmission, the TX applies an $N_{\text{tx}} \times 1$ phase shift vector $\mathbf{f}[n]$ to its phased array. As $\mathbf{f}[n]$ is realized using phase shifters, it must be chosen such that $\sqrt{N_{\text{tx}}}\mathbf{f}[n] \in \mathbb{Q}_{\text{tx}}^{N_{\text{tx}}}$. At the receiver, the stream of signals at the N_{rx} antennas are combined using $\mathbf{w}[n]$ such that $\sqrt{N_{\text{rx}}}\mathbf{w}[n] \in \mathbb{Q}_{\text{rx}}^{N_{\text{rx}}}$. It can be observed that each of the vectors $\mathbf{f}[n]$ and $\mathbf{w}[n]$ have unit norm. In this work, we assume perfect frame timing and carrier synchronization. Extension of this work for low-complexity compressive beam alignment in uniform planar arrays can be found in [13]. The focus of [13], however, is more on the design of CS matrices that achieve robustness to carrier frequency offset. With the perfect synchronization assumption, the received symbol for the n^{th} pilot transmission can be expressed as

$$\tilde{y}[n] = \mathbf{w}^T[n]\mathbf{H}\mathbf{f}[n]t[n] + \tilde{v}[n], \tag{1}$$

where $\tilde{v}[n] \sim \mathcal{CN}(0, \sigma^2)$ is additive white Gaussian noise. As the pilot symbols are known to the RX, the channel measurements can be computed as $y[n] = \tilde{y}[n]/t[n]$. The channel measurements are then

$$y[n] = \mathbf{w}^T[n]\mathbf{H}\mathbf{f}[n] + v[n], \tag{2}$$

where $v[n]$ has the same statistics as that of $\tilde{v}[n]$ since $|t[n]| = 1$. It can be observed from (2) that each channel measurement is a projection of the MIMO channel onto a matrix that is determined by the weights applied to the phased array.

To model the mmWave MIMO channel matrix, we consider a geometric-ray-based model with K rays [14]. For the k^{th} ray, we use γ_k to denote the complex ray gain. We use $\theta_{\text{tx},k}$ and $\theta_{\text{rx},k}$ to denote the angle-of-departure (AoD) and the angle-of-arrival (AoA) of the k^{th} ray. We define the $N \times 1$ Vandermonde vector as

$$\mathbf{a}_N(\Delta) = [1, e^{j\Delta}, e^{j2\Delta}, ..., e^{j(N-1)\Delta}]^T. \tag{3}$$

Using these definitions, the $N_{\text{rx}} \times N_{\text{tx}}$ MIMO channel matrix between the TX and the RX is

$$\mathbf{H} = \sum_{k=1}^{K} \gamma_k \mathbf{a}_{N_{\text{rx}}}(\theta_{\text{rx},k})\mathbf{a}_{N_{\text{tx}}}^T(\theta_{\text{tx},k}). \tag{4}$$

At mmWave carrier frequencies, $\mathbf{H}$ in (4) is approximately sparse in the 2D-DFT basis [2]. We use $\mathbf{X} \in \mathbb{C}^{N_{\text{rx}} \times N_{\text{tx}}}$ to denote the 2D-DFT representation of $\mathbf{H}$ as

$$\mathbf{H} = \mathbf{U}_{N_{\text{rx}}}\mathbf{X}\mathbf{U}_{N_{\text{tx}}}. \tag{5}$$

The matrix $\mathbf{X}$, called as the beamspace channel, is not exactly sparse due to leakage effects that arise from the use of finite angle domain dictionaries [6]. For our analysis, we ignore such leakage effects and assume that $\mathbf{X}$ is perfectly sparse. Our simulations, however, include these effects as our training solution is evaluated for realistic mmWave channels.

III. Spatial Zadoff-Chu modulation for CS

The constant amplitude and zero autocorrelation properties of Zadoff-Chu sequences [11] have been well exploited along the time and frequency dimensions in wireless systems, but not in space. To the best of our knowledge, [15] is the only work that used ZC sequences in space for compressive channel estimation. The efficiency of ZC-based CS matrices in terms of the RIP or incoherence, however, was not characterized in [15]. In this work, we show that such CS matrices satisfy the RIP and aid low complexity CS algorithms.

We define a convolutional channel acquisition framework where the channel measurements are obtained by applying circulant shifts of a pair of core ZC sequences to the phased arrays at the TX and the RX. The k^{th} element of a ZC sequence $\mathbf{b} \in \mathbb{C}^N$ is given as

$$b[k] = \begin{cases} \frac{1}{\sqrt{N}}\exp\left(\text{j}\frac{\pi u k(k+1)}{N}\right), & \text{if } N \text{ is odd} \\ \frac{1}{\sqrt{N}}\exp\left(\text{j}\frac{\pi u k^2}{N}\right), & \text{if } N \text{ is even} \end{cases}. \tag{6}$$

The integer u in (6) must be co-prime with N and is defined as the root of the ZC sequence [11]. Let $\mathbf{f} \in \mathbb{C}^{N_{\text{tx}}}$ and $\mathbf{w} \in \mathbb{C}^{N_{\text{rx}}}$ be the core ZC sequences used by the TX and the RX for the convolutional acquisition. To model the circulant shifts, we define circulant delay matrices $\mathbf{J}_{N_{\text{tx}}} \in \mathbb{C}^{N_{\text{tx}} \times N_{\text{tx}}}$ and $\mathbf{J}_{N_{\text{rx}}} \in \mathbb{C}^{N_{\text{rx}} \times N_{\text{rx}}}$. The first row of $\mathbf{J}_{N_{\text{tx}}}$ is $(0, 1, 0, 0, ..., 0)$. The subsequent rows of $\mathbf{J}_{N_{\text{tx}}}$ are generated by circulantly shifting the previous row to the right by 1 unit. For example,

$\mathbf{J}_3$ in compact form is $[\mathbf{e}_2, \mathbf{e}_0, \mathbf{e}_1]$. Using this definition, we define a d-circulant delay matrix $\mathbf{J}_{N_{\rm tx},d} = \mathbf{J}_{N_{\rm tx}}\mathbf{J}_{N_{\rm tx}}...\mathbf{J}_{N_{\rm tx}}$ (d times). Note that $\mathbf{J}_{N_{\rm tx},1} = \mathbf{J}_{N_{\rm tx}}$, and $\mathbf{J}_{N_{\rm tx},0}$ is an identity matrix of size $N_{\rm tx} \times N_{\rm tx}$. The matrices $\mathbf{J}_{N_{\rm rx}}$ and $\mathbf{J}_{N_{\rm rx},d}$ are defined in a similar way. It can be observed that for any vector $\mathbf{p} \in \mathbb{C}^{N_{\rm tx}}$, the vector $\mathbf{J}_{N_{\rm tx},d}\mathbf{p}$ is a right-circulantly shifted version of $\mathbf{p}$ by d units.

The proposed convolutional training is defined by the vectors $\mathbf{f}$ and $\mathbf{w}$, and the circulant shift pairs $\{(r[n], c[n])\}_{n=1}^{N_{\rm p}}$. Each pair $(r[n], c[n])$ contains the integers $r[n] \in \mathcal{I}_{N_{\rm rx}}$ and $c[n] \in \mathcal{I}_{N_{\rm tx}}$. For the $n^{\rm th}$ channel measurement, the TX circulantly shifts $\mathbf{f}$ to the right by $c[n]$ units, and applies the resultant vector to the phased array. In compact form, the weight vector applied to the phased array at the TX is $\mathbf{f}[n] = \mathbf{J}_{N_{\rm tx},c[n]}\mathbf{f}$. The RX receives the pilot symbol by combining the signals from its antennas using a $r[n]$ circulantly shifted version of $\mathbf{w}$, i.e., $\mathbf{w}[n] = \mathbf{J}_{N_{\rm rx},r[n]}\mathbf{w}$. Under the convolutional acquisition framework, the channel measurements in (2) can be expressed as

$$y[n] = \mathbf{w}^T\mathbf{J}_{N_{\rm rx},r[n]}^T\mathbf{H}\mathbf{J}_{N_{\rm tx},c[n]}\mathbf{f} + v[n] \tag{7}$$

$$= \mathbf{w}^T\mathbf{J}_{N_{\rm rx},r[n]}^T\mathbf{U}_{N_{\rm rx}}\mathbf{X}\mathbf{U}_{N_{\rm tx}}\mathbf{J}_{N_{\rm tx},c[n]}\mathbf{f} + v[n] \tag{8}$$

$$= (\mathbf{U}_{N_{\rm rx}}\mathbf{J}_{N_{\rm rx},r[n]}\mathbf{w})^T\mathbf{X}\mathbf{U}_{N_{\rm tx}}\mathbf{J}_{N_{\rm tx},c[n]}\mathbf{f} + v[n]. \tag{9}$$

It can be observed that (8) follows from (7) using the sparse 2D-DFT representation of $\mathbf{H}$ in (5). The simplification in (9) follows from the symmetry of the DFT matrix, i.e., $\mathbf{U}_{N_{\rm rx}} = \mathbf{U}_{N_{\rm rx}}^T$. Now, we prove a lemma that will be useful to obtain a partial 2D-DFT equation out of (9).

Lemma 1. *For any vector $\mathbf{z} \in \mathbb{C}^N$ and a diagonal matrix $\mathbf{\Lambda_z} = \sqrt{N}\mathrm{diag}(\mathbf{U}_N\mathbf{z})$ that contains the DFT of $\mathbf{z}$, we have*

$$\mathbf{U}_N\mathbf{J}_{N,d}\mathbf{z} = \mathbf{\Lambda_z}\mathbf{U}_N\mathbf{e}_d. \tag{10}$$

Proof. Let $\tilde{\mathbf{z}}$ be the N point DFT of the sequence $\mathbf{z}$, i.e., $\tilde{\mathbf{z}} = \mathbf{U}_N\mathbf{z}$. The DFT duality between $\mathbf{z}$ and $\tilde{\mathbf{z}}$ is often represented using $z[\ell] \longleftrightarrow \tilde{z}[k]$, where $\ell \in \mathcal{I}_N$ and $k \in \mathcal{I}_N$ denote the time and frequency indices. From the shifting property of the DFT, it follows that [16]

$$z[(\ell - d) \bmod N] \longleftrightarrow \tilde{z}[k]e^{-2\pi dk/N}. \tag{11}$$

It can be noticed from (11) that a circulant shift of d units in the time domain signal induces a phase gradient that is proportional to d in the frequency domain signal. In vector notation, the DFT of $\mathbf{J}_{N,d}\mathbf{z}$, the d circulant shifted version of $\mathbf{z}$, can be expressed using (11) as

$$\mathbf{U}_N\mathbf{J}_{N,d}\mathbf{z} = \tilde{\mathbf{z}} \odot (1, e^{-\mathrm{j}2\pi d/N}, e^{-\mathrm{j}4\pi d/N}, .., e^{-\mathrm{j}2\pi d(N-1)/N})^T. \tag{12}$$

It can be observed from (12) that the vector that induces the phase gradients in the DFT is a scaled version of the $d^{\rm th}$ column of the DFT, i.e.,

$$(1, e^{-\mathrm{j}2\pi d/N}, e^{-\mathrm{j}4\pi d/N}, .., e^{-\mathrm{j}2\pi d(N-1)/N})^T = \sqrt{N}\mathbf{U}_N\mathbf{e}_d. \tag{13}$$

From (12) and (13), we can write

$$\mathbf{U}_N\mathbf{J}_{N,d}\mathbf{z} = \sqrt{N}\tilde{\mathbf{z}} \odot \mathbf{U}_N\mathbf{e}_d. \tag{14}$$

Using $\tilde{\mathbf{z}} = \mathbf{U}_N\mathbf{z}$ and the relation $\mathbf{p} \odot \mathbf{q} = \mathrm{diag}(\mathbf{p})\mathbf{q}$, we can rewrite (14) as $\mathbf{U}_N\mathbf{J}_{N,d}\mathbf{z} = \sqrt{N}\mathrm{diag}(\mathbf{U}_N\mathbf{z})\mathbf{U}_N\mathbf{e}_d$. The result in Lemma 1 now follows from the definition of $\mathbf{\Lambda_z}$. □

Now, we prove that the channel measurement in (9) can be interpreted as a 2D-DFT sample of a masked beamspace matrix. We define $\mathbf{\Lambda_f} = \sqrt{N_{\rm tx}}\mathrm{diag}(\mathbf{U}_{N_{\rm tx}}\mathbf{f})$ and $\mathbf{\Lambda_w} = \sqrt{N_{\rm rx}}\mathrm{diag}(\mathbf{U}_{N_{\rm rx}}\mathbf{w})$. For the $n^{\rm th}$ channel measurement, the DFTs of the weight vectors at the TX and the RX can be expressed as

$$\mathbf{U}_{N_{\rm tx}}\mathbf{J}_{N_{\rm tx},c[n]}\mathbf{f} = \mathbf{\Lambda_f}\mathbf{U}_{N_{\rm tx}}\mathbf{e}_{c[n]} \text{ and} \tag{15}$$

$$\mathbf{U}_{N_{\rm rx}}\mathbf{J}_{N_{\rm rx},r[n]}\mathbf{w} = \mathbf{\Lambda_w}\mathbf{U}_{N_{\rm rx}}\mathbf{e}_{r[n]} \tag{16}$$

using the result in Lemma 1. From (9), (15) and (16), the $n^{\rm th}$ channel measurement can be written as

$$y[n] = \mathbf{e}_{r[n]}^T\mathbf{U}_{N_{\rm rx}}\mathbf{\Lambda_w}\mathbf{X}\mathbf{\Lambda_f}\mathbf{U}_{N_{\rm tx}}\mathbf{e}_{c[n]} + v[n]. \tag{17}$$

We define the masked beamspace matrix as $\mathbf{S} = \mathbf{\Lambda_w}\mathbf{X}\mathbf{\Lambda_f}$. The channel measurement in (17) is then

$$y[n] = \mathbf{e}_{r[n]}^T\mathbf{U}_{N_{\rm rx}}\mathbf{S}\mathbf{U}_{N_{\rm tx}}\mathbf{e}_{c[n]} + v[n]. \tag{18}$$

It can be observed from (18) that the channel measurement is a noisy version of the $(r[n], c[n])$ sample of the 2D-DFT of the masked beamspace $\mathbf{S}$. Specifically, the noiseless $y[n]$ is the $(2\pi r[n]/N_{\rm rx}, 2\pi c[n]/N_{\rm tx})$ spatial frequency component of $\mathbf{S}$ [17]. An important observation from the spectral mask equation, i.e., $\mathbf{S} = \mathbf{\Lambda_w}\mathbf{X}\mathbf{\Lambda_f}$, is that $\mathbf{S}$ is sparse whenever $\mathbf{X}$ is sparse due to the diagonal nature of $\mathbf{\Lambda_w}$ and $\mathbf{\Lambda_f}$. Using different circulant shifts at the TX and the RX, it can be noticed from (18) that several 2D-DFT samples of $\mathbf{S}$ can be acquired. As partial Fourier matrices are known to satisfy the RIP, the masked beamspace matrix can be efficiently obtained from the channel measurements [12].

Convolutional channel acquisition using generic phase shift vectors $\mathbf{f}$ and $\mathbf{w}$ does not guarantee the recovery of $\mathbf{X}$ even when $\mathbf{S}$ is successfully recovered from its partial 2D-DFT measurements. It is because the spectral mask matrices $\mathbf{\Lambda_w}$ and $\mathbf{\Lambda_f}$ may not be invertible for any $\mathbf{f}$ and $\mathbf{w}$. When the spectral mask matrices are invertible, the true beamspace estimate can be recovered from the masked beamspace estimate as $\mathbf{X} = \mathbf{\Lambda_w}^{-1}\mathbf{S}\mathbf{\Lambda_f}^{-1}$. For the special case when $\mathbf{f}$ and $\mathbf{w}$ are unit-norm Zadoff-Chu sequences, we prove in Sec. IV that the spectral masks are perfectly conditioned and obtain guarantees on the recovery of $\mathbf{X}$ from sub-Nyquist channel measurements.

IV. RIP OF SHIFTED ZC-BASED CS MATRIX

In this section, we translate recovery guarantees from partial DFT-CS of $\mathbf{S}$ to that of CCS of $\mathbf{H}$ with random shifted-ZC sequences. We use $\Omega = \{(r[n], c[n])\}_{n=1}^{N_{\rm p}}$ to denote an ordered set of $N_{\rm p}$ distinct coordinates chosen uniformly at random from $\mathcal{I}_{N_{\rm rx}} \times \mathcal{I}_{N_{\rm tx}}$. Using the $n^{\rm th}$ coordinate in Ω, the channel measurement $y[n]$ is obtained by using circulant shifts of $r[n]$ and $c[n]$ at the RX and the TX. We define a projection operator $\mathcal{P}_\Omega : \mathbb{C}^{N_{\rm rx} \times N_{\rm tx}} \to \mathbb{C}^{N_{\rm p}}$ that returns the entries of an $N_{\rm rx} \times N_{\rm tx}$ matrix at the locations in Ω. It can be observed from (18) that the $N_{\rm p}$ channel measurements defined by Ω are samples of the

2D-DFT of $\mathbf{S}$ at the locations in Ω. The vector $\mathbf{y}$ that contains the $N_{\rm p}$ channel measurements is

$$\mathbf{y} = \mathcal{P}_{\Omega}(\mathbf{U}_{N_{\rm rx}}\mathbf{S}\mathbf{U}_{N_{\rm tx}}) + \mathbf{v}. \tag{19}$$

We define the ℓ_1 norm of a matrix as $\|\mathbf{P}\|_{\ell_1} = \sum_{k,\ell} |\mathbf{P}(k,\ell)|$. The matrix $(\mathbf{P})_k$ is used to denote the k sparse representation of $\mathbf{P}$, and is obtained from $\mathbf{P}$ by retaining its k largest entries in magnitude and setting the rest to 0.

The sparse masked beamspace matrix $\mathbf{S}$ can be recovered from $\{y[n]\}_{n=1}^{N_{\rm p}}$ using the ℓ_1 norm minimization program [3]

$$\hat{\mathbf{S}} = \begin{array}{c} \arg\min \ \|\mathbf{G}\|_{\ell_1} \\ \mathbf{G} \\ \text{s.t } \|\mathbf{y} - \mathcal{P}_{\Omega}\left(\mathbf{U}_{N_{\rm rx}}\mathbf{G}\mathbf{U}_{N_{\rm tx}}\right)\|_2 \leq \sqrt{N_{\rm p}}\sigma \end{array}. \tag{20}$$

The reconstruction guarantee for the sparse masked beamspace estimate obtained using (20) is summarized in Theorem 1.

Theorem 1. *For a fixed constant $\eta \in (0,1)$, if $N_{\rm p} \geq Ck \max\left\{\log^3(2k)\log(N_{\rm tx}N_{\rm rx}), \log(\eta^{-1})\right\}$ then the solution to* (20) *satisfies*

$$\left\|\mathbf{S} - \hat{\mathbf{S}}\right\|_F \leq C_1 \frac{\|\mathbf{S} - (\mathbf{S})_k\|_{\ell_1}}{\sqrt{k}} + C_2\sqrt{N_{\rm tx}N_{\rm rx}}\sigma, \tag{21}$$

with a probability of at least $1-\eta$. The constants C, C_1 and C_2 are independent of all the other parameters.

Proof. The result follows from Theorems 1 and 3 of [18]. □

The bound in (21) follows from the restricted isometry property of partial 2D-DFT matrices. It can be observed from (21) that a sparse approximation of the masked beamspace matrix can be recovered with $\mathcal{O}(\log(N_{\rm tx}N_{\rm rx}))$ channel measurements.

When the spectral masks are invertible, the true beamspace is estimated as $\hat{\mathbf{X}} = \mathbf{\Lambda}_{\mathbf{w}}^{-1}\hat{\mathbf{S}}\mathbf{\Lambda}_{\mathbf{f}}^{-1}$. In this case, $\|\mathbf{X} - \hat{\mathbf{X}}\|_F = \|\mathbf{\Lambda}_{\mathbf{w}}^{-1}(\mathbf{S} - \hat{\mathbf{S}})\mathbf{\Lambda}_{\mathbf{w}}^{-1}\|_F$. When $\mathbf{f}$ and $\mathbf{w}$ are unit-norm ZC sequences, it can be shown that their DFTs, i.e., $\mathbf{U}_{N_{\rm tx}}\mathbf{f}$ and $\mathbf{U}_{N_{\rm rx}}\mathbf{w}$ are also unit-norm ZC sequences [19]. By the constant magnitude property of the ZC sequence, every entry of the vector $\mathbf{U}_{N_{\rm tx}}\mathbf{f}$ has magnitude $1/\sqrt{N_{\rm tx}}$, and every entry of $\mathbf{U}_{N_{\rm rx}}\mathbf{w}$ has magnitude $1/\sqrt{N_{\rm rx}}$. Therefore, the diagonal entries of the matrices $\mathbf{\Lambda}_{\mathbf{f}}$ and $\mathbf{\Lambda}_{\mathbf{w}}$ have unit magnitude whenever $\mathbf{f}$ and $\mathbf{w}$ are ZC sequences. As a result, we have $\|\mathbf{X} - \hat{\mathbf{X}}\|_F = \|\mathbf{S} - \hat{\mathbf{S}}\|_F$. Furthermore, it can be shown that $\|\mathbf{X} - (\mathbf{X})_k\|_{\ell_1} = \|\mathbf{S} - (\mathbf{S})_k\|_{\ell_1}$. For the conditions in Theorem 1, the norm preserving property of ZC spectral masks can be used in (21) to obtain

$$\left\|\mathbf{X} - \hat{\mathbf{X}}\right\|_F \leq C_1 \frac{\|\mathbf{X} - (\mathbf{X})_k\|_{\ell_1}}{\sqrt{k}} + C_2\sqrt{N_{\rm tx}N_{\rm rx}}\sigma. \tag{22}$$

The MIMO channel is estimated as $\hat{\mathbf{H}} = \mathbf{U}_{N_{\rm rx}}\hat{\mathbf{X}}\mathbf{U}_{N_{\rm tx}}$. Note that the upper bound in (22) also applies for the MIMO channel estimation error, i.e., $\|\mathbf{H} - \hat{\mathbf{H}}\|_F$, due to the unitary nature of the DFT matrices.

An important point to be noted is that several random CS matrices that satisfy the RIP with high probability, and guarantee the recovery of sparse signals cannot be realized in mmWave hardware. In phased arrays, the failure to realize such matrices is due to the inability to perform amplitude control over the signals at every antenna. For instance, IID Gaussian CS matrices, that are known to satisfy the RIP, cannot be realized with phase shifters. Similarly, partial DFT CS matrices cannot be directly realized as they require antenna switching [13]. In contrast, the ℓ_1 norm minimization program with random shifted-ZC sequences guarantees the recovery of mmWave channel matrices for sub-Nyquist sampling. We have derived these guarantees using the uniform DFT property of the ZC sequence, and by proving the equivalence of CCS with partial 2D-DFT CS.

CS algorithms that use the proposed training have a lower computational complexity than those that use random IID phase shifts. For example, in standard CS problems of the form $\mathbf{y} = \mathbf{A}\mathbf{s} + \mathbf{v}$, many iterative CS algorithms require computing $\mathbf{A}\mathbf{p}$ and $\mathbf{A}^*\mathbf{r}$ in every iteration. The vectors $\mathbf{p}$ and $\mathbf{r}$ correspond to the sparse estimate and the corresponding measurement residual in an iteration. For the special case in (19) where the CS measurements are partial 2D-DFT projections of a sparse matrix, the vectors $\mathbf{A}\mathbf{p}$ and $\mathbf{A}^*\mathbf{r}$ can be computed efficiently using the fast Fourier transform [18].

V. Beam alignment in wideband mmWave systems

We consider an L tap wideband MIMO channel $\{\mathbf{H}[\ell]\}_{\ell=0}^{L-1}$ and describe how to use the proposed ZC-based training for wideband channels. To obtain channel measurements using the proposed ZC-based training, $N_{\rm p}$ distinct coordinates $\{(r[n], c[n])\}_{n=1}^{N_{\rm p}}$ are sampled uniformly at random from $\mathcal{I}_{N_{\rm rx}} \times \mathcal{I}_{N_{\rm tx}}$. For the $n^{\rm th}$ spatial channel measurement, phase shift vectors $\mathbf{J}_{N_{\rm tx},c[n]}\mathbf{f}$ and $\mathbf{J}_{N_{\rm rx},r[n]}\mathbf{w}$ are applied at the TX and the RX. For the wideband case, a low aperiodic autocorrelation (LAAC) sequence of length N_s followed by $L-1$ zeros is transmitted by the TX over each of the $N_{\rm p}$ phase shift configurations. The signalling scheme is shown in Fig. 2. The zero padding in the frame structure prevents inter-frame interference, and allows sufficient time to configure the phase shifters [7]. It is assumed that the settling time of phase shifters is smaller than $L-1$ symbol durations. When LAAC sequences of desirable length do not exist, complementary sequences of appropriate length can be used in the frame structure. For simplicity of exposition, we assume that a good LAAC sequence of length $N_{\rm s}$ exists.

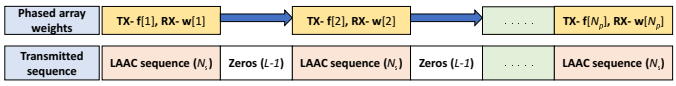

Fig. 2. In this frame structure, a zero padded low aperiodic autocorrelation (LAAC) sequence is transmitted for each phase shift configuration.

The RX correlates the received signal with the same LAAC sequence used by the TX and obtains the channel impulse response (CIR) seen with the $n^{\rm th}$ phase shift configuration. The CIR for the $n^{\rm th}$ phase shift configuration is a vector of length L and is denoted by $\mathbf{y}[n] \in \mathbb{C}^L$. Using the frame structure in Fig. 2, the CIR for $N_{\rm p}$ different phase shift configurations can be obtained in $N_{\rm p}(N_{\rm s} + L - 1)$ symbol

durations. We define a matrix $\mathbf{Y} = [\mathbf{y}[1], \mathbf{y}[2], ..., \mathbf{y}[N_\mathrm{p}]]$ that contains a collection of CIRs seen for N_p distinct phase shift configurations. The block of measurements, i.e., $\mathbf{Y}$, can be processed for CS-based wideband channel estimation. The complexity of the channel estimation problem, however, is at least L times higher than the beam alignment problem.

As the focus of our work is on beam alignment, we develop a low complexity approach that selects a single row of $\mathbf{Y}$ with the maximum norm. Let $\mathbf{y}_b \in \mathbb{C}^{N_\mathrm{p}}$ be the b^{th} row vector that has the maximum norm among the L rows of $\mathbf{Y}$. The channel measurements in $\mathbf{y}_b$ are compressive spatial projections of $\mathbf{H}[b]$, the MIMO channel corresponding to the b^{th} tap. We use $\mathbf{H}[m]$ to denote the MIMO channel tap that has the maximum energy of the L taps. In practice, $\mathbf{H}[b]$ can be different from $\mathbf{H}[m]$ as b is determined from lower-dimensional spatial projections of the L MIMO channel taps. Let $\hat{\mathbf{H}}[b]$ be the estimate of $\mathbf{H}[b]$ obtained using a CS algorithm over $\mathbf{y}_b$. In this work, we use orthogonal matching pursuit (OMP) [20], a greedy CS algorithm, to estimate $\mathbf{H}[b]$ from $\mathbf{y}_b$. The matrix $\hat{\mathbf{H}}[b]$ obtained from OMP can be considered as an equivalent narrowband channel estimate that is used for beam alignment.

Now, we describe the procedure for beam alignment using the single tap channel estimate obtained from OMP. Beam alignment is performed using the top singular vectors, i.e., the singular vectors that correspond to the maximum value, in the singular value decomposition (SVD) of $\hat{\mathbf{H}}[b]$. Let $\mathbf{w}_{\mathrm{uq}}$ be the conjugate of the top left singular vector of $\hat{\mathbf{H}}[b]$. We define $\mathbf{f}_{\mathrm{uq}}$ as the top right singular vector of $\hat{\mathbf{H}}[b]$. Although these vectors maximize $|\mathbf{p}^T\hat{\mathbf{H}}[b]\mathbf{q}|$ for any pair of unit norm vectors $\mathbf{p} \in \mathbb{C}^{N_{\mathrm{rx}}}$ and $\mathbf{q} \in \mathbb{C}^{N_{\mathrm{tx}}}$, they cannot be applied in phased arrays. Nevertheless, $\mathbf{f}_{\mathrm{uq}}$ and $\mathbf{w}_{\mathrm{uq}}$ can be projected onto the feasible sets for beam alignment. The projection $\mathbf{f}_{\mathrm{est}}$ is derived by quantizing the phase of every element of $\mathbf{f}_{\mathrm{uq}}$ according to $\mathbb{Q}_{\mathrm{tx}}$, and by setting its entry-wise magnitude to $1/\sqrt{N_{\mathrm{tx}}}$. Similarly, the projection $\mathbf{w}_{\mathrm{est}}$ is derived from $\mathbf{w}_{\mathrm{uq}}$ using $\mathbb{Q}_{\mathrm{rx}}$. The vectors $\mathbf{f}_{\mathrm{est}}$ and $\mathbf{w}_{\mathrm{est}}$ are applied as beamforming weights to the phased arrays at the TX and the RX. The performance of CS algorithm is determined by the achievable rate observed after beam alignment, which is the capacity of the L-tap wideband SISO channel $\left\{\mathbf{w}_{\mathrm{est}}^T\mathbf{H}[\ell]\mathbf{f}_{\mathrm{est}}\right\}_{\ell=0}^{L-1}$. To benchmark the performance of the CS algorithm, we evaluate the maximum achievable rate in a similar manner using the best beam alignment vectors $\mathbf{w}_{\mathrm{opt}}$ and $\mathbf{f}_{\mathrm{opt}}$. The vectors $\mathbf{w}_{\mathrm{opt}}$ and $\mathbf{f}_{\mathrm{opt}}$ are obtained using the SVD of the actual maximum energy tap $\mathbf{H}[m]$, followed by projection of the singular vectors onto the feasible set.

VI. Simulations

We consider a phased array system in Fig. 1 with $N_{\mathrm{tx}} = 32$ and $N_{\mathrm{rx}} = 16$ antennas. The resolution of the phase shifters at the TX and the RX was set to $q_{\mathrm{tx}} = 3$ bits and $q_{\mathrm{rx}} = 2$ bits. The operating bandwidth of the mmWave system was $B = 100\,\mathrm{MHz}$ at a carrier frequency of $28\,\mathrm{GHz}$ [21]. The wideband MIMO channel used in our simulations was derived from the NYU channel simulator [22] for a NLoS scenario in an urban micro environment. The wideband channel $\{\mathbf{H}[\ell]\}_{\ell=0}^{L-1}$ was scaled so that $\mathbb{E}[\sum_{\ell\in\mathcal{I}_L}\|\mathbf{H}[\ell]\|_F^2] = N_{\mathrm{rx}}N_{\mathrm{tx}}$. The SNR in the system is defined as $\mathrm{SNR} = 10\log_{10}(1/\sigma^2)$. The distance between the TX and the RX was set to $60\,\mathrm{m}$. For simulations, we used $L = 13$ taps to model the wideband mmWave channel. The number of taps chosen is reasonable as the omnidirectional RMS delay spread for most channel realizations at $28\,\mathrm{GHz}$ was observed to be much smaller than $L/W = 130\,\mathrm{ns}$, i.e., the duration of the CIR considered for 13 taps and $100\,\mathrm{MHz}$ [13][22].

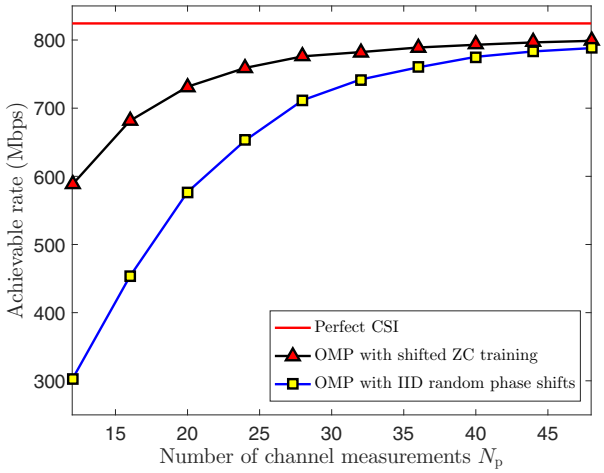

Fig. 3. For an SNR of $0\,\mathrm{dB}$, the plot shows the achievable data rate as a function of the number of channel measurements, i.e., N_p. The shifted ZC-based training performs better than the IID phase shift-based training for any N_p.

For beam alignment with the ZC-based training, the core sequence at the TX, i.e., $\mathbf{f}$, was chosen as a ZC sequence with root 11 and length 32. The core sequence $\mathbf{w}$ at the RX was chosen as another ZC sequence with root 9 and length 16. The roots of $\mathbf{f}$ and $\mathbf{w}$ were adjusted empirically so that their q_{tx} and q_{rx} bit quantized versions result in unimodular DFTs. The channel measurements are obtained using the frame structure in Fig. 2 for N_p different phase shift configurations at the TX and the RX. A Barker sequence [23] of length $N_\mathrm{s} = 13$ was used as the LAAC sequence in our simulations. For the parameters used in our simulations, the guard interval for each configuration is $(L-1)/B = 120\,\mathrm{ns}$. The guard interval is sufficient enough as phase shifters with a settling time of about $30\,\mathrm{ns}$ at $28\,\mathrm{GHz}$ have been reported in [24]. Beam alignment is performed using random shifted ZC-based training via OMP for 100 channel realizations and 50 random ZC-based realizations for each channel realization. The achievable rate that we report is the average over all these realizations. The duration of channel acquisition for N_p measurements is $N_\mathrm{p}(N_\mathrm{s}+L-1)/B$. For exhaustive scanning techniques, the duration would be $N_{\mathrm{rx}}N_{\mathrm{tx}}(N_\mathrm{s}+L-1)/B$. The performance of compressive beam alignment using the proposed training is shown in Fig. 3 for different values of N_p at an SNR of $0\,\mathrm{dB}$. It can be observed that $N_\mathrm{p} = 24$,

which is about 5% of $N_{\mathrm{rx}}N_{\mathrm{tx}}$, channel measurements suffice to achieve good rates using the proposed training.

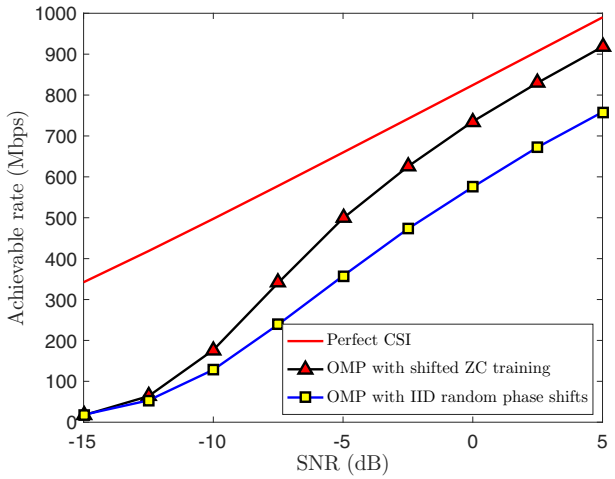

Fig. 4. The plot shows the achievable data rate as a function of SNR for a channel acquisition duration of 5 μs, i.e., $N_{\mathrm{p}} = 20$. Shifted ZC-based training is advantageous over IID phase shift training at all levels of SNR.

For a benchmark, we compute the maximum achievable rate defined in Sec. V using the MIMO channel tap with the maximum Frobenius norm. This maximum achievable rate corresponds to the perfect channel state information (CSI) scenario. We also evaluate the beam alignment performance when OMP is used with channel measurements generated using IID random phase shifts at the TX and the RX [5]. It can be observed from Fig. 3 and Fig. 4 that the proposed ZC-based training outperforms the IID random phase shift training under the same settings. For instance, at an SNR= $0\,\mathrm{dB}$ and $N_{\mathrm{p}} = 20$, beam alignment using our training guarantees data rates that are about $150\,\mathrm{Mbps}$ higher than that obtained with the IID phase shift-based training.

VII. Conclusions and Future Work

In this work, we have developed a new approach for compressed sensing in phased antenna arrays using Zadoff-Chu modulation in the antenna domain. We have shown the equivalence between convolutional CS and partial DFT CS for signals that are sparse in the Fourier domain. Using the equivalence and the properties of the ZC sequence, we derived guarantees on MIMO channel reconstruction from sub-Nyquist channel measurements. We have shown that the proposed shifted ZC-based training performs better beam alignment than the commonly used random phase shift training. In our future work, we will design ZC-like sequences that can be implemented with ultra-low resolution phase shifters.

VIII. Acknowledgement

This research was partially supported by the National Science Foundation under Grant No. NSF-CNS-1702800 and by the U.S. Department of Transportation through the Data-Supported Transportation Operations and Planning (D-STOP) Tier 1 University Transportation Center.

References

[1] S. Rangan, T. S. Rappaport, and E. Erkip, "Millimeter-wave cellular wireless networks: Potentials and challenges," *in Proc. of the IEEE*, vol. 102, no. 3, pp. 366–385, 2014.

[2] R. W. Heath, N. Gonzalez-Prelcic, S. Rangan, W. Roh, and A. M. Sayeed, "An overview of signal processing techniques for millimeter wave MIMO systems," *IEEE J. Sel. Topics Signal Process.*, vol. 10, no. 3, pp. 436–453, 2016.

[3] E. J. Candès and M. B. Wakin, "An introduction to compressive sampling," *IEEE Signal Process. Mag.*, vol. 25, no. 2, pp. 21–30, 2008.

[4] J. Brady, N. Behdad, and A. M. Sayeed, "Beamspace MIMO for millimeter-wave communications: System architecture, modeling, analysis, and measurements," *IEEE Trans. Antennas and Propagation*, vol. 61, no. 7, pp. 3814–3827, 2013.

[5] A. Alkhateeb, G. Leus, and R. W. Heath, "Compressed sensing based multi-user millimeter wave systems: How many measurements are needed?" in *Proc. of the IEEE Int. Conf. Acoust., Speech Signal Process.(ICASSP)*, 2015, pp. 2909–2913.

[6] Z. Marzi, D. Ramasamy, and U. Madhow, "Compressive channel estimation and tracking for large arrays in mm-wave picocells," *IEEE J. Sel. Topics Signal Process.*, vol. 10, no. 3, pp. 514–527, 2016.

[7] J. Rodríguez-Fernández, N. González-Prelcic, K. Venugopal, and R. W. Heath Jr, "Frequency-domain compressive channel estimation for frequency-selective hybrid mmWave MIMO systems," *IEEE Trans. Wireless Commun.*, vol. 17, no. 5, pp. 2946–2960, 2018.

[8] K. Li, L. Gan, and C. Ling, "Convolutional compressed sensing using deterministic sequences," *IEEE Trans. Signal Process.*, vol. 61, no. 3, pp. 740–752, 2013.

[9] H. Rauhut, "Circulant and toeplitz matrices in compressed sensing," in *Proc. of Signal. Process. with Adapt. Sparse Structured Repn. (SPARS)*, 2009.

[10] J.-M. Feng, F. Krahmer, and R. Saab, "Quantized compressed sensing for partial random circulant matrices," in *Proc. of Intl. Conf. on Sampl. Theory and Appln. (SampTA)*, 2017, pp. 236–240.

[11] D. Chu, "Polyphase codes with good periodic correlation properties," *IEEE Trans. Inform. Theory*, vol. 18, no. 4, pp. 531–532, 1972.

[12] E. J. Candès, J. Romberg, and T. Tao, "Robust uncertainty principles: Exact signal reconstruction from highly incomplete frequency information," *IEEE Trans. Inform. Theory*, vol. 52, no. 2, pp. 489–509, 2006.

[13] N. J. Myers, A. Mezghani, and R. W. Heath Jr, "Swift-link: A compressive beam alignment algorithm for practical mmwave radios," *arXiv preprint arXiv:1806.02005*, 2018.

[14] R. Heath, *Introduction to Wireless Digital Communication: A Signal Processing Perspective*. Pearson Education, 2017.

[15] Y. Ding, S.-E. Chiu, and B. D. Rao, "Bayesian channel estimation algorithms for massive MIMO systems with hybrid analog-digital processing and low resolution adcs," *IEEE J. Sel. Topics Signal Process.*, 2018.

[16] A. V. Oppenheim and R. W. Schafer, "Discrete-time signal processing," 2010.

[17] A. C. Kak and M. Slaney, *Principles of computerized tomographic imaging*. IEEE press, 1998.

[18] F. Krahmer and H. Rauhut, "Structured random measurements in signal processing," *GAMM-Mitteilungen*, vol. 37, no. 2, pp. 217–238, 2014.

[19] M. M. Mansour, "Optimized architecture for computing Zadoff-Chu sequences with application to LTE," in *Proc. of the IEEE Global Telecommun. Conf. (GLOBECOM)*, 2009, pp. 1–6.

[20] J. A. Tropp and A. C. Gilbert, "Signal recovery from random measurements via orthogonal matching pursuit," *IEEE Trans.on Inform. theory*, vol. 53, no. 12, pp. 4655–4666, 2007.

[21] F. B. Mismar and B. L. Evans, "Machine learning approach to estimating mmWave signal measurements during handover," *arXiv preprint arXiv:1710.01879*, 2017.

[22] S. Sun, G. R. MacCartney Jr, and T. S. Rappaport, "A novel millimeter-wave channel simulator and applications for 5G wireless communications," *arXiv preprint arXiv:1703.08232*, 2017.

[23] S. Golomb and R. Scholtz, "Generalized Barker sequences," *IEEE Trans. on Inform. Theory*, vol. 11, no. 4, pp. 533–537, 1965.

[24] M. E. Leinonen, G. Destino, O. Kursu, M. Sonkki, and A. Prssinen, "28 GHz wireless backhaul transceiver characterization and radio link budget," *ETRI Journal*, vol. 40, no. 1, 2018.